

# Crystallization phenomena in bacterial poly[(*R*)-3-hydroxybutyrate]: 3. Toughening via texture changes

G. J. M. de Koning\*, A. H. C. Scheeren and P. J. Lemstra

Centre for Polymers and Composites (CPC), Eindhoven University of Technology,  
PO Box 513, 5600 MB Eindhoven, The Netherlands

and M. Peeters and H. Reynaers

Department of Chemistry, University of Leuven, Celestijnenlaan 200 F, B 3001 Heverlee,  
Belgium

(Received 12 January 1994; revised 11 April 1994)

Poly[(*R*)-3-hydroxybutyrate] (PHB) is a bacterial storage polyester that is genuinely biodegradable, but its brittleness hampers its wide applicability as a biodegradable plastic. Most attempts to improve the mechanical properties of PHB have focused on incorporating comonomers, but at the expense of production costs. Strikingly, it appeared possible to toughen PHB homopolymer using a simple annealing treatment. The present study attributes this remarkable phenomenon to a change in the lamellar morphology, which reduces the amorphous-crystalline interface area and thus the constraint imposed on the amorphous chains by the crystals. This elevates the relaxation strength of the amorphous regions, giving rise to the favourable fracture behaviour.

(Keywords: poly(hydroxybutyrate); crystallization; toughening)

## INTRODUCTION

Poly[(*R*)-3-hydroxybutyrate] (PHB) is a biopolymer accumulated by bacteria as a reserve of carbon and energy<sup>1,2</sup>. Owing to its natural origin, PHB can be biodegraded by a wide variety of micro-organisms<sup>3,4</sup>. Since PHB is a hydrophobic and thermoplastic polyester, it might be ideal as a biodegradable plastic<sup>5</sup>. In 1982, Zeneca developed a process for the industrial production of PHB using the bacterium *Alcaligenes eutrophus* grown on glucose. Owing to its enzymatic synthesis, PHB has an exceptional stereochemical purity. The chains are linear and the chiral centres all possess the *R* stereochemical configuration<sup>6</sup>. As a consequence, the polymer is completely isotactic and capable of crystallizing.

A major drawback of PHB is its brittleness, which seriously limits its application possibilities. Although as-moulded PHB shows ductile behaviour, upon storage at ambient temperature an ageing process embrittles the material. Our previous results showed that this remarkable embrittlement is an intrinsic property of the polymer<sup>7</sup> and should be attributed to secondary crystallization<sup>8</sup>. Up to now, most attempts to overcome the brittleness of PHB have focused on incorporating comonomers. For example, PHB copolymers with 3-hydroxyvalerate have been commercialized by Zeneca<sup>5</sup> under the trademark Biopol™. These copolymers are obtained by using specific additives in the growth medium of the bacteria. Notwithstanding

the superior mechanical properties of the copolymers<sup>9</sup>, their production costs are higher than for the homopolymer since the required additives<sup>10</sup> are expensive. Moreover, the presence of comonomer affects the crystallization kinetics of the polymer<sup>11-13</sup>, giving rise to longer processing cycle times.

Alternatively, we recently demonstrated<sup>8</sup> that, using a simple annealing treatment, PHB homopolymer can be toughened while subsequent ageing is prevented to a large extent. Annealing at a temperature of 110°C increased the elongation at break from 5% to over 25%, an observation that is particularly surprising since annealing usually embrittles a semicrystalline polymer. The present study aims to explain this remarkable phenomenon.

## EXPERIMENTAL

### Materials

The PHB homopolymer investigated was a Biopol™ sample ( $M_w = 539 \text{ kg mol}^{-1}$ ,  $M_w/M_n = 3.5$ ,  $T_m = 174^\circ\text{C}$ ), provided by Zeneca BioProducts as a fine powder. The powder was mixed with 1 wt% boron nitride in a Hobart mixer for approximately 10 min. Boron nitride acts as a nucleating agent<sup>14</sup> to enhance the otherwise slow crystallization process. Moreover, the presence of a consistent concentration of nucleating agent is essential in order to eliminate any variation of the spherulite size and concomitant mechanical effects.

\* To whom correspondence should be addressed. Present address: Institute for Biotechnology, ETH Hönggerberg, 8093 Zürich, Switzerland

### Sample preparation

The powder mixture was extruded into a single 4 mm diameter strand using a Betol 2520 extruder (diameter 25 mm; filters 60 and 100 mesh) operated at a maximum of 180°C and at a screw speed of 100 rev min<sup>-1</sup>. The strand was crystallized in a 60°C water bath and pelletized. The pellets were injection-moulded using a Boy 15S injection-moulding machine. Processing specifications were as follows: maximum barrel temperature 155°C; injection time 15 s; screw speed 250 rev min<sup>-1</sup>; injection pressure 4 MPa; mould temperature 60°C; cooling time 15 s. Melt processing reduced the PHB molar mass ( $M_w$ ) from 539 to 309 kg mol<sup>-1</sup> ( $M_w/M_n=2.9$ ). The injection-moulded specimens were dumbbell-shaped according to ISO R 537/2, their prismatic part measuring 40 × 5.3 × 1.9 mm<sup>3</sup>. The samples were stored for 10 days at ambient temperature and subsequently annealed in a hot-air oven (Heraeus) at temperatures ranging from 90 to 150°C and for periods ranging from 10 to 1225 min. To assure a uniform temperature, the samples were placed between two metal plates, the temperature of which was monitored by means of a thermocouple connected to the plates. Since an ageing process is known to affect the annealed material at an early stage<sup>8</sup>, all specimens were stored for 20 days under ambient conditions prior to characterization.

### Characterization techniques

**Tensile testing.** Tensile testing was performed at ambient conditions using a Frank 81565. A clamp separation of 50 mm and a crosshead speed of 20 mm min<sup>-1</sup> were used. For each set of annealing conditions, four samples were tested.

**Dynamic mechanical thermal analysis.** Dynamic mechanical measurements were performed with a Polymer Laboratories dynamic Mechanical Analyser operated in the single cantilever bending mode. Injection-moulded specimens (1.9 × 5.3 × 12 mm<sup>3</sup>) were investigated at a measuring frequency of 1 Hz and a heating rate of 2°C min<sup>-1</sup>.

**Differential scanning calorimetry.** Melting endotherms were recorded using a Perkin-Elmer DSC-7 differential scanning calorimeter. Indium was used for temperature and heat-of-fusion calibration. Mass fraction crystallinities could be calculated from the melting peak area, assuming that the heat of fusion of 100% crystalline PHB<sup>15</sup> amounts to 146 J g<sup>-1</sup>.

**Density measurements.** In order to measure the density of a PHB sample, a piece of the specimen was immersed into a range of aqueous potassium bromide solutions. In order to assure optimal wetting, 0.03% of a detergent was added. The solutions were thermostatically controlled at 22.5°C and their concentrations were chosen such that their densities ranged from 1.225 to 1.257 g cm<sup>-3</sup> with intervals of 0.00064 g cm<sup>-3</sup>. The sample density reported is the average of the density of the solution in which the sample just floated and that of the solution in which it just sunk. The density of PHB,  $\rho_{\text{PHB}}$ , was obtained by correcting the sample density for the presence of 1 wt% boron nitride (BN):

$$\rho_{\text{PHB}} = 0.99 \times \frac{\rho_{\text{sample}}}{1 - 0.01(\rho_{\text{sample}}/\rho_{\text{BN}})}$$

where  $\rho_{\text{BN}} = 2.25 \text{ g cm}^{-3}$ . Densities could be translated into the volume fraction and the mass fraction crystallinities,  $X_v$  and  $X_m$  respectively, using:

$$X_v = \frac{\rho_{\text{PHB}} - \rho_a}{\rho_{\text{cr}} - \rho_a} \quad X_m = X_v \frac{\rho_{\text{cr}}}{\rho_{\text{PHB}}}$$

with density of amorphous phase<sup>15</sup>  $\rho_a = 1.179 \text{ g cm}^{-3}$  and density of crystalline phase<sup>15</sup>  $\rho_{\text{cr}} = 1.279 \text{ g cm}^{-3}$ .

**Transmission electron microscopy.** Pieces of injection-moulded samples were trimmed ready for microtoming and subsequently treated during 16 h with a 2% ruthenium tetroxide solution at room temperature. Thin sections were obtained by ultramicrotomy at ambient temperature using a Reichert Ultracut E Microtome. The thin sections (thickness 100 nm) were stained in ruthenium tetroxide vapour for 2 h at room temperature. Transmission electron microscopy was performed using a JEOL JEM 2000 FX microscope operated at 80 kV.

**Small-angle X-ray scattering.** SAXS measurements were conducted at ambient temperature with a Rigaku-type Kratky camera using infinite slit geometry. Ni-filtered Cu K<sub>α</sub> radiation was produced using a Rigaku rotating-anode device operated at 50 kV and 150 mA. The sample-to-detector distance was 280 mm. Each sample had a thickness of 1.9 mm and was exposed for 30 min. Scattering patterns were collected with a linear position-sensitive detector (Braun OED-SOM). All relevant parameters describing the lamellar morphology, as listed in Figure 1, were computed from the obtained scattering data according to the Vonk model<sup>16</sup> using the FFSAXS-5 program<sup>17</sup>.

From applying different but reasonable fitting ranges, the standard deviations for the morphological parameters were estimated to be 3 Å. Within this accuracy, identical results were obtained when the lamellar thickness was simply derived from the product  $X_v L$  (see Figure 8). The

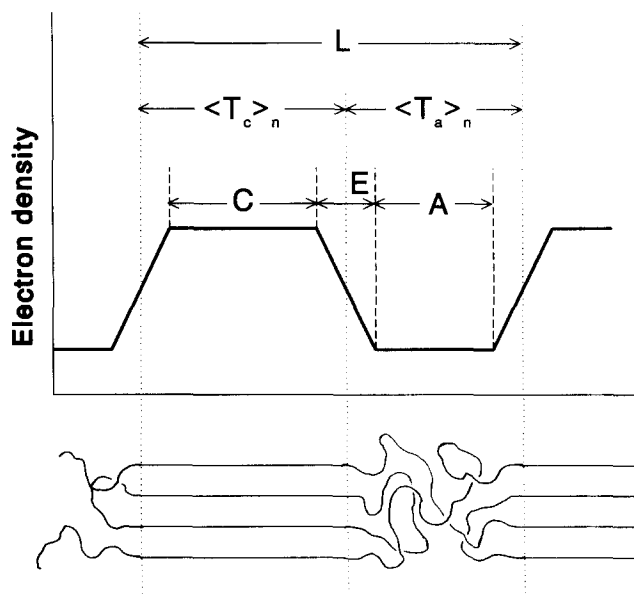


**Figure 1** Schematic presentation of the lamellar morphology, perpendicular to the lamellae, and the corresponding electron density profile according to the pseudo-two-phase model described by Vonk<sup>16</sup>:  $L$  = periodicity,  $\langle T_c \rangle_n$  = lamellar thickness,  $\langle T_a \rangle_n$  = amorphous thickness,  $C$  = lamellar core,  $A$  = amorphous core,  $E$  = transition layer

latter method goes with an ideal two-phase model where the phase boundary is assumed to be infinitely sharp. This similarity implies that PHB does not contain any amorphous regions apart from those in the lamellar stacks.

## RESULTS

### Previous results in retrospect

In the preceding paper<sup>8</sup> in this series it was argued that the remarkable embrittlement of moulded PHB should be attributed to secondary crystallization, which tightly constrains the amorphous phase. The latter was concluded from the changes in the dynamic mechanical characteristics, which reflect a loss of the relaxation strength, i.e. the pliability, of the amorphous phase. In a

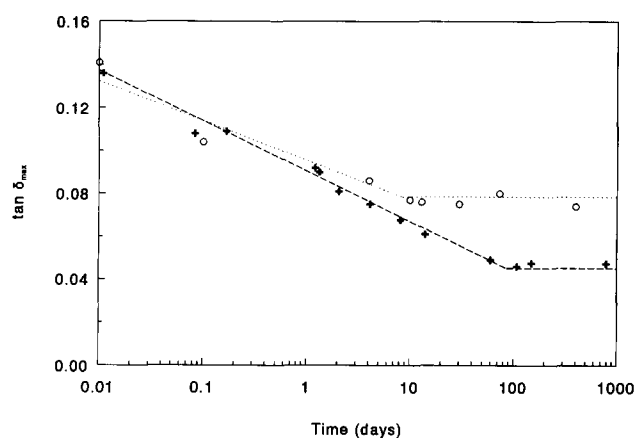


**Figure 2** Dynamic loss peak maximum versus time of storage at room temperature for as-moulded PHB (+) and for PHB annealed for 16h at 110°C (O)

creep experiment, this relaxation strength is defined as the normalized difference in strain between the initial unrelaxed state and the final relaxed state. For the case of a standard linear solid, it can be demonstrated that both the drop in storage modulus at the glass transition and the dynamic loss peak maximum ( $\tan \delta_{\max}$ ) scale with this relaxation strength<sup>18</sup>.  $\tan \delta_{\max}$  is closest to the original definition of relaxation strength in being normalized to a dimensionless quantity. Also in real polymer systems,  $\tan \delta_{\max}$  is an appropriate, though not proportional, measure of the relaxation strength.

When  $\tan \delta_{\max}$  is monitored during storage of a moulded PHB sample using the previous data<sup>8</sup>, this quantity shows a logarithmic decrease with time until it stabilizes at ca. 100 days (Figure 2). Accordingly, the tensile modulus and Izod impact strength show a logarithmic change with time and deterioration ceases after some 100 days<sup>8</sup>. A similar parallel between the relaxation strength of the amorphous phase and the macroscopic mechanical properties is observed<sup>8</sup> for PHB annealed at 110°C. After annealing,  $\tan \delta_{\max}$  initially decreases similarly as in as-moulded material, but soon stabilizes at a higher level (Figure 2). Accordingly, deterioration is minor and is apparently complete after only a few days.

In the sequel, this favourable toughening effect upon annealing will be studied by comparing the ultimate materials, i.e. after deterioration has ceased.

### Mechanical changes upon annealing

Injection-moulded PHB samples were annealed at different conditions and subsequently stored at room temperature. The sample densities were determined 20 days (Table 1) and 80 days after annealing. Identical

**Table 1** Characteristics of moulded PHB annealed for different times  $t_a$  at different temperatures  $T_a$

$T_a$ (°C)	$t_a$ (min)	$\rho_{\text{PHB}}$ ( $\pm 0.0003 \text{ g cm}^{-3}$ )	$X_{m,\rho}$ ( $\pm 0.3\%$ )	$X_{m,\Delta H}$ ( $\pm 4\%$ )	$\tan \delta_{\max}$ ( $\pm 0.001$ )	$\epsilon_b$ (%)
Original	0	1.2375	60.4	58	0.043	5.3 ( $\pm 0.4$ )
95	10	1.2393	62.3	58	0.053	9.0 ( $\pm 0.7$ )
	30	1.2406	63.5	61	0.058	10.3 ( $\pm 1.1$ )
	60	1.2412	64.1	62	0.057	9.3 ( $\pm 0.5$ )
	120	1.2418	64.7	66	0.060	12.0 ( $\pm 1.2$ )
	750	1.2418	64.7	66	0.057	14.2 ( $\pm 1.8$ )
115	10	1.2418	64.7	60	0.061	17.3 ( $\pm 2.5$ )
	30	1.2418	64.7	65	0.066	22.5 ( $\pm 2.6$ )
	60	1.2431	65.9	63	0.066	19.8 ( $\pm 3.7$ )
	150	1.2437	66.5	66	0.070	24.7 ( $\pm 4.1$ )
	350	1.2443	67.1	68	0.067	21.7 ( $\pm 0.5$ )
	1225	1.2449	67.7	68	0.067	10.0 ( $\pm 0.8$ )
128	10	1.2431	65.9	65	0.065	25.5 ( $\pm 8.5$ )
	30	1.2443	67.1	65	0.070	30.4 ( $\pm 1.3$ )
	60	1.2443	67.1	66	0.069	25.5 ( $\pm 5.4$ )
147	3	1.2443	67.1	68	–	18.0 ( $\pm 4.2$ )
	10	1.2449	67.7	66	0.069	26.0 ( $\pm 5.6$ )
	30	1.2462	68.9	66	0.069	26.5 ( $\pm 8.1$ )

$\rho_{\text{PHB}}$  Sample density corrected for the presence of 1 wt% boron nitride

$X_{m,\rho}$  Mass fraction crystallinity calculated from density

$X_{m,\Delta H}$  Mass fraction crystallinity calculated from d.s.c. melt enthalpy

$\tan \delta_{\max}$  Dynamic loss peak maximum (measuring frequency: 1 Hz)

$\epsilon_b$  Elongation at break (draw rate: 50%  $\text{min}^{-1}$ )

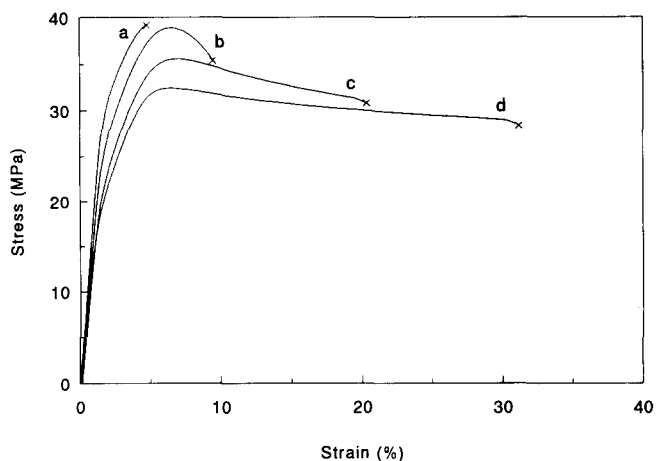


**Figure 3** Stress-strain curves of moulded PHB samples annealed for (a) 0 min, (b) 60 min at 95°C, (c) 60 min at 115°C and (d) 30 min at 128°C

results were obtained, which verifies the previous observation<sup>8</sup> that the ageing process in annealed PHB is completed within 20 days. The data show that annealing gave rise to an increase in density, which is likely to be attributed to an increase in crystallinity. This assumption was verified by the increase in the d.s.c. melting endotherm area. Although d.s.c. is not as accurate as density measurements, the crystallinities calculated from both methods correspond well (Table 1).

An increase in crystallinity generally results in an increase in modulus. Surprisingly, tensile testing (Figure 3) demonstrated the opposite. The modulus decreased slightly despite the increase in crystallinity. At the same time, the elongation at break  $\epsilon_b$  rose from 5% up to as much as 30% (Figure 3 and Table 1). (Upon annealing for a very long time, e.g. 1225 min at 115°C, the material deteriorated due to degradation, as was evident from a change in the sample colour.)

Consistent with the results from tensile testing, above  $T_g$  the dynamic storage modulus dropped below that of the non-annealed sample (Figure 4). Similarly, annealing raised  $\tan \delta_{\max}$  in spite of the decrease in amorphous fraction. Both trends indicate that the relaxation strength of the remaining amorphous chains must have increased significantly.

#### Morphological changes upon annealing

Figure 5 presents the crystal morphologies of PHB before and after annealing as viewed by TEM. It clearly shows that the lamellar crystals are grouped in stacks and that annealing increased the lamellar thickness. The lamellar texture of the original material was found to be exceptionally fine compared to that of other semi-crystalline polymers, showing a periodicity as small as 70 Å. Annealing produced a much coarser lamellar texture comparable to that of polypropylene. Consistent quantitative results were obtained from the SAXS measurements. Upon annealing the Bragg reflection shifted to lower angles (Figure 6A), which implies an increase in the periodicity. The corresponding correlation functions are presented in Figure 6B. All correlation functions showed well pronounced maxima, indicative of a regular stacking of the lamellae. Again, lamellar thickening is obvious, as the wavelength equals the periodicity  $L$ . Table 2 clearly demonstrates that the rate

and the significance of the thickening process increased with the annealing temperature.

Bulk crystallinities and correlation functions were combined to give the average lamellar thickness  $\langle T_c \rangle_n$  and amorphous thickness  $\langle T_a \rangle_n$  (Table 2) according to the pseudo-two-phase model. The width of the transition layer ( $E$ ) was found to be more or less constant and amounted to  $12 \pm 1.5$  Å (Table 2), which can be speculated to be close to the dimensions of the fold region.

#### Structural reorganization

In view of the data in Table 2, which show a wide variety of lamellar thicknesses, the corresponding thermograms (Figure 7) are surprising. A peak melting temperature of  $174 \pm 2^\circ\text{C}$  was observed for all samples, which is completely inconsistent with the established fact that the melting point increases with the lamellar thickness. Obviously, the peak maximum of the endotherm does not represent the melting temperature of the original crystals. Recent studies<sup>11-13</sup> related this observation to a rearrangement of the initial crystal morphology. Upon heating, the crystals experience a continuous melting and structural reorganization into thicker and more stable crystals, which therefore have higher melting temperatures. The peak temperature only indicates the point at which the net difference between melting and recrystallization passes through a maximum.

More evidence for the occurrence of such a rearrangement process was furnished by the SAXS results. Table 2 shows that annealing gave rise to a considerable increase in lamellar thickness accompanied by only a slight increase in crystallinity. Similarly, annealing appeared to thicken both  $\langle T_c \rangle_n$  and  $\langle T_a \rangle_n$ . These observations exclude simple core thickening, which would be at the expense of  $\langle T_a \rangle_n$ , and imply that the total number of crystals was reduced. Therefore, some

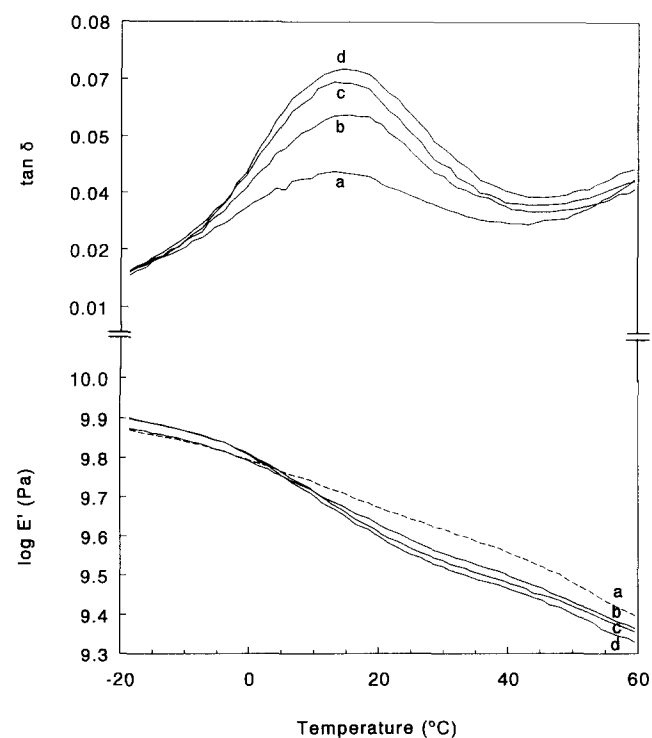


**Figure 4** Dynamic mechanical spectra of moulded PHB samples annealed for (a) 0 min, (b) 60 min at 95°C, (c) 60 min at 115°C and (d) 10 min at 147°C

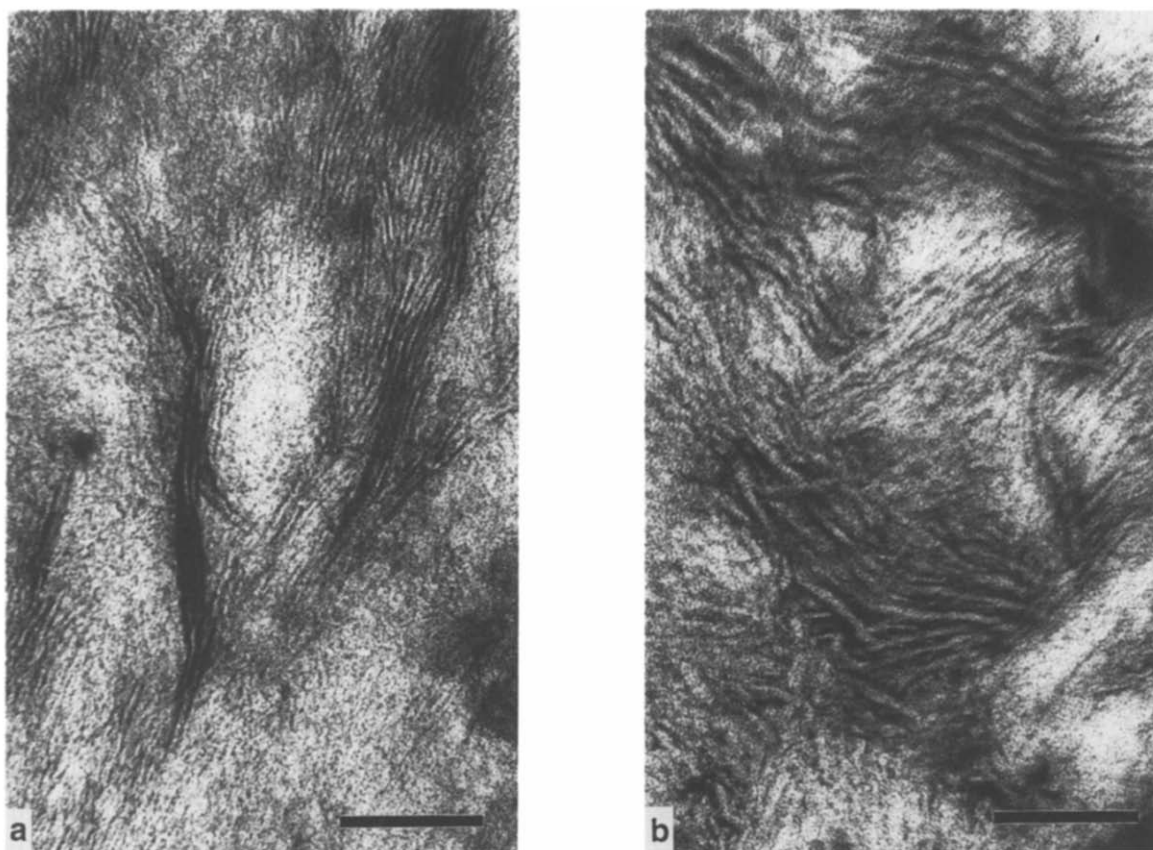


Figure 5 TEM micrographs of moulded PHB samples annealed for (a) 0 min and (b) 10 min at 147°C (scale bar: 1000 Å)

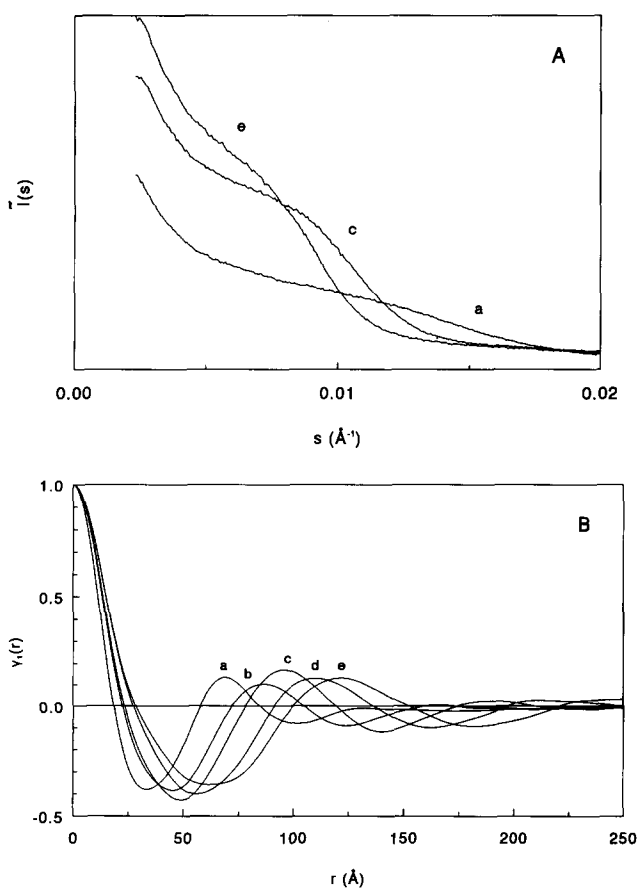


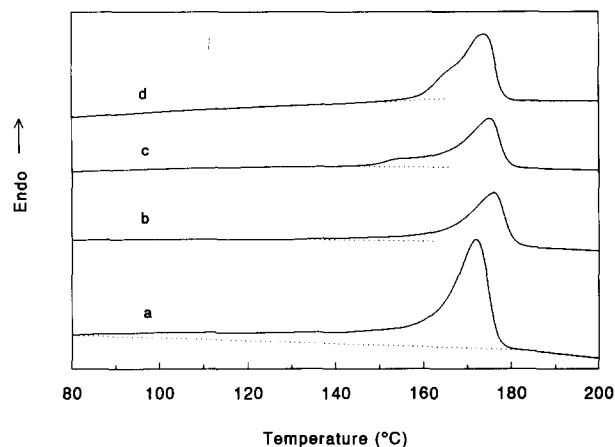
Figure 6 Smear scattering curves (A) and correlation functions (B) of moulded PHB samples annealed for (a) 0 min, (b) 60 min at 95°C, (c) 60 min at 115°C, (d) 30 min at 128°C and (e) 10 min at 147°C

Table 2 Morphological characteristics of moulded PHB that was annealed for different times  $t_a$  at different temperatures  $T_a$  (morphological parameters are depicted in Figure 1; standard deviation:  $\pm 3$  Å)

$T_a$ (°C)	$t_a$ (min)	$X_v$ (%)	$L$ (Å)	$E$ (Å)	$\langle T_c \rangle_n$ (Å)	$C$ (Å)	$\langle T_a \rangle_n$ (Å)	$A$ (Å)
Original	0	58.5	69	11	41	30	29	18
95	10	60.3	80	11	49	38	32	22
	30	61.6	83	12	53	41	33	22
	60	62.2	87	11	55	44	34	23
	120	62.8	87	11	54	43	32	22
	750	62.8	86	11	55	44	33	22
115	10	62.8	96	11	61	49	36	25
	30	62.8	98	12	61	49	36	25
	60	64.1	97	12	61	50	35	23
	150	64.7	99	11	63	51	35	23
	350	65.3	102	12	69	57	37	25
	1225	65.9	102	13	67	54	35	23
128	10	64.1	107	13	69	56	39	26
	30	65.3	110	13	72	59	38	26
	60	65.3	111	13	71	58	38	25
147	3	65.3	108	12	66	55	36	24
	10	65.9	124	14	77	63	40	26
	30	67.1	128	14	81	67	40	26

melting and recrystallization must have occurred. The relations of  $\langle T_c \rangle_n$  and  $\langle T_a \rangle_n$  versus the periodicity  $L$  (Figure 8) appeared to be uniform and linear, which indicates that it is the same mechanism operating at all annealing conditions.

In order to get a notion of the rate of the rearrangement process, thermograms of non-annealed PHB were recorded at different heating rates (Figure 9). A small sample



**Figure 7** Thermograms (heating rate  $20^{\circ}\text{C min}^{-1}$ ) of moulded PHB samples annealed for (a) 0 min, (b) 60 min at  $115^{\circ}\text{C}$ , (c) 30 min at  $128^{\circ}\text{C}$  and (d) 10 min at  $147^{\circ}\text{C}$

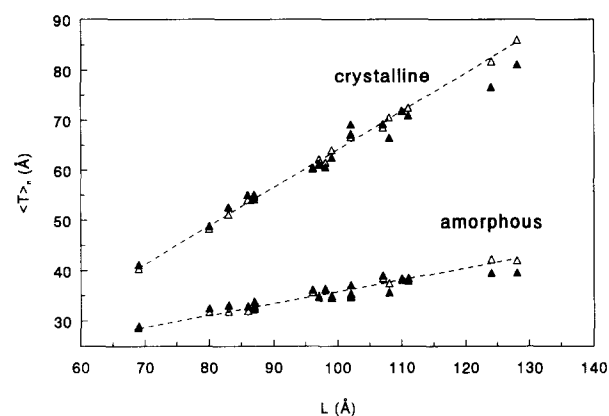


**Figure 8** Average crystalline and amorphous thickness of annealed PHB versus the periodicity  $L$  calculated according to the ideal two-phase model ( $\Delta$ ) and the pseudo-two-phase model ( $\blacktriangle$ )

mass (0.5 mg) was used to minimize thermal lag. At higher heating rates, the lower-temperature part of the endotherm became increasingly visible. Obviously, upon rapid heating, reorganization had less time to occur, resulting in net melting. The lower end of the endotherm, which indicates the onset of melting of the most unstable crystals, appeared as low as  $80^{\circ}\text{C}$ . Moreover, an additional peak developed at  $165^{\circ}\text{C}$ , which may represent the melting of the most stable crystals of the initial morphology. These results suggest that the initial crystal morphology of PHB crystallized at  $60^{\circ}\text{C}$  consists of crystals with melting points ranging from  $80$  to  $165^{\circ}\text{C}$ . This variety can be explained by postulating that crystals are formed with a wide range of defect concentrations. Most crystals are relatively perfect, but the defect concentration in some crystals is such that they are only just stable at the crystallization temperature.

The foregoing implies that rapid heating to an annealing temperature over  $80^{\circ}\text{C}$  will give rise to an initial reduction of the crystallinity. Indeed, there is evidence of true melting at these low temperatures<sup>12,13</sup>. From the ultimate gain in crystallinity (Table 1) it is obvious that subsequent recrystallization occurs at the annealing temperature. Of course, the more perfect and thus still intact crystals will act as nuclei for recrystallization. In other words, the defective crystals disappear

in favour of thickening of the more perfect lamellae. The formation of more perfect crystalline material upon annealing could be observed from the thermograms (Figure 7). The onset of melting was always just about  $15^{\circ}\text{C}$  above the annealing temperature, and at increasing annealing times this onset developed into a pronounced shoulder.

Comparing these results with previous studies<sup>11,13,15</sup> on the effect of crystallization temperature, a striking similarity was observed. PHB annealed at a certain temperature gave a thermogram and periodicity similar to a sample crystallized at the same temperature. This resemblance suggests that both annealing and crystallizing would yield identical textures if performed at the same temperature. This does not seem unrealistic in respect of the concept of melting and recrystallization upon annealing. Attempts to verify this hypothesis failed, because the crystallization rate of PHB above  $120^{\circ}\text{C}$  is almost negligible<sup>11</sup>. Therefore, long crystallization times were required, giving rise to considerable degradation.

## DISCUSSION

### Relating the relaxation strength

From the results from both the ageing<sup>8</sup> and rejuvenation experiments, it is evident that  $\tan \delta_{\text{max}}$ , representing the relaxation strength of the amorphous phase, is a most important indicator in studying the toughness of PHB. Changes in  $\tan \delta_{\text{max}}$  can be caused by variation of either the amorphous fraction or the constraint in the amorphous regions. The latter obviously plays a dominant role in the case of PHB, since the changes in crystallinity are relatively minor. In conclusion, changes in the constraint imposed on the amorphous phase consistently give rise to corresponding changes in macroscopic toughness.

Notably, the morphology is not an indicator of the mechanical properties. Both as-moulded and as-annealed PHB show similar toughness<sup>8</sup> but possess very different morphologies. Moreover, during subsequent ageing the morphology has been found to be constant<sup>8</sup>. Even so, the morphology does determine the ultimate properties by governing to what extent ageing occurs. Figure 3 clearly shows that ageing of as-moulded PHB, which has been shown to have an extremely fine lamellar morphology, is much more dramatic than that of annealed PHB, which exhibits a coarser morphology.

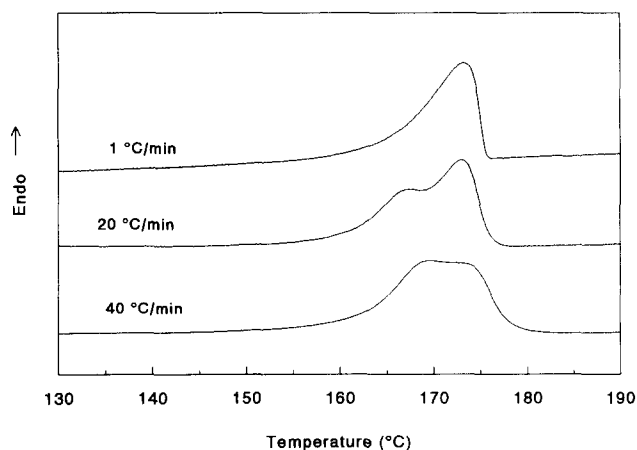


**Figure 9** Thermograms of moulded PHB at different heating rates

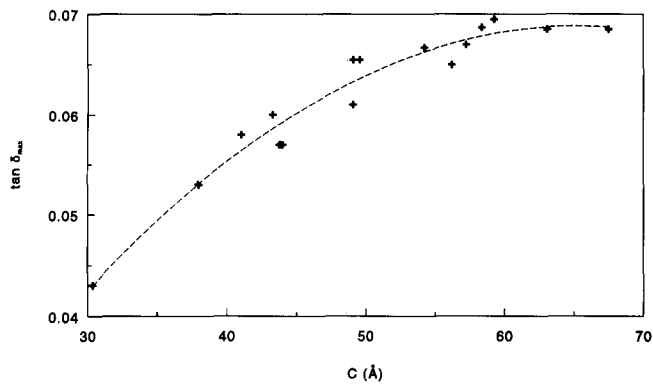


**Figure 10** Ultimate loss peak maximum ( $\tan \delta_{\max}$ ) versus the crystal core thickness ( $C$ ) for annealed PHB

Using the lamellar core thickness  $C$  as an arbitrary parameter representing the morphology, *Figure 10* shows the relationship between the ultimate relaxation strength of the amorphous phase and the morphology.

#### Role of morphology

In the previous section, annealing has been shown to rearrange PHB crystals by a process of melting and recrystallization. Therefore, both as-moulded and as-annealed PHB may be regarded as if crystallized from the melt, but at different supercoolings. Accordingly, annealing increases and may even double the periodicity (*Table 2*). Implicitly, the crystalline–amorphous interface per unit volume, which is proportional to the reciprocal periodicity, may decrease by some factor 2.

Both as-moulded and as-annealed PHB initially show similar high relaxation strengths, i.e. their amorphous phase is 'loose' (*Figure 2*). In the previous paper<sup>8</sup>, it was argued that the subsequent constraining of the amorphous phase upon ageing should be attributed to secondary crystallization. The observation<sup>8</sup> that the morphology is constant throughout ageing specifies secondary crystallization as crystal perfection<sup>19</sup>, which may involve rectifying the chain conformation and thickening of the crystal core. The latter simply consists of perfection processes in the crystalline–amorphous interface at the expense of the amorphous layer, e.g. the rearrangement of loops in the fold region. The resulting constraint imposed on the amorphous regions will be lower in annealed material, since annealing reduces the ratio of interface area to amorphous material. This forms the basis for the relationship observed between the morphology and the ultimate relaxation strength (*Figure 10*). Notably, the volume of material involved in crystal perfection, i.e. the total amount of interface material, decreases upon annealing. Consistently, the increase in density (crystallinity) upon ageing in as-moulded material is much higher than that in annealed material<sup>8</sup>.

#### Mechanism of deformation

A direct consequence of the elevated relaxation strength of the amorphous phase in the annealed material is the somewhat lower elastic modulus (*Figure 3*), since generally the amorphous phase almost entirely accounts for the elastic part of the deformation<sup>20</sup> between  $T_g$  and  $T_m$ . However, *Figure 3* demonstrates that it is the ability to undergo plastic deformation that is responsible for the toughness of annealed PHB. Semicrystalline polymers

generally<sup>20</sup> deform plastically by slip in the crystals. However, polymer crystals rarely possess the five independent slip systems necessary for a general change of their shape, as must occur in the deformation of a polycrystalline aggregate. In order to enable plastic deformation, it is therefore essential that the amorphous regions between adjacent crystals allow a certain amount of adjustment to accommodate some rotation of the crystals. Apparently, the amorphous regions in the non-annealed PHB are too constrained for this. Upon distortion the amorphous chains tighten up immediately, and break at their failure stress, producing a brittle fracture. Annealing elevates the relaxation strength of the amorphous chains, thus allowing more relative motion of the amorphous regions between crystals. The pliability of the amorphous phase then may become sufficient to allow plastic deformation before the chain failure stress is reached.

The concept postulated above is consistent with the observed parallel between  $\tan \delta_{\max}$ , representing the relaxation strength of the amorphous phase, and the macroscopic strain at break ( $\epsilon_b$ ). When plotting  $\epsilon_b$  versus  $\tan \delta_{\max}$ , indeed a reasonable relation was obtained. However, the results from ageing<sup>8</sup> and annealing experiments yielded separate relations (*Figure 11*). Apparently,  $\tan \delta_{\max}$  is not the only factor determining the macroscopic mechanical properties. Since it is not unlikely that the dimensions of crystalline and amorphous regions affect the deformation behaviour, the involvement of various morphological parameters was evaluated. Surprisingly, the discrepancy appeared to be largely smoothed out by involving the interlamellar distance  $A$  (*Figure 12*). This

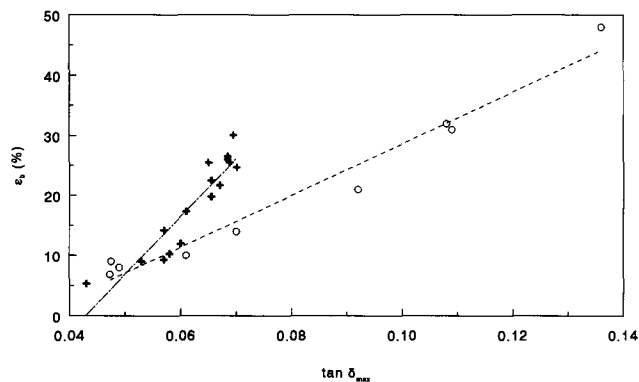


**Figure 11** Elongation at break ( $\epsilon_b$ ) versus the loss peak maximum ( $\tan \delta_{\max}$ ) from ageing ( $\circ$ ) and annealing experiments ( $+$ )

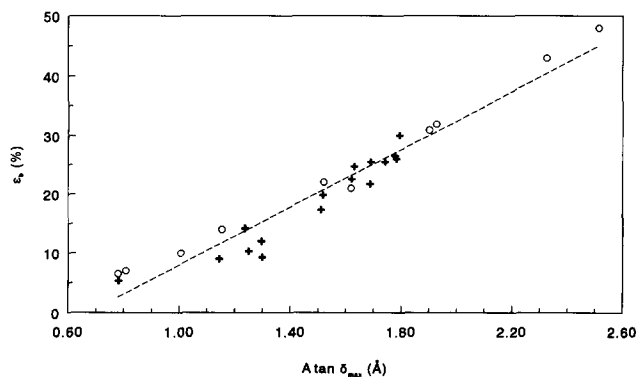


**Figure 12** Elongation at break ( $\epsilon_b$ ) versus  $A \tan \delta_{\max}$  from ageing ( $\circ$ ) and annealing experiments ( $+$ )

arbitrary act even largely eliminated the scattering in the plot.

Apparently, the deformation behaviour can be completely described by involving the relaxation strength of the amorphous parts and some morphological parameter, preferably though arbitrarily the interlamellar distance  $A$ . One possible explanation of this remarkable observation is that a critical adjustment of the interlamellar gap is required to enable plastic deformation. Since the relaxation strength relates to a (normalized) strain, the absolute adjustment of an amorphous region will scale with both its relaxation strength and the interlamellar distance  $A$ . Therefore, the plastic deformation mechanism may operate only at these locations in the material where the product  $A \tan \delta_{\max}$  exceeds the critical value. *Figure 12* does not exhibit the step usually associated with a critical value, because both  $A$  and  $\tan \delta_{\max}$  are the means of distributions of values corresponding to the numerous amorphous regions. Upon intensifying the annealing conditions, an increasing fraction of the amorphous regions becomes sufficiently compliant to allow rotation of the adjacent crystals, i.e. the number of sites suited for local plastic deformation increases, giving rise to a gradual increase in the macroscopic strain at break.

## CONCLUSIONS

It has been demonstrated that, using a simple annealing treatment, brittle PHB homopolymer can be toughened. Annealing a PHB sample at 150°C suffices to achieve an ultimate extension at break of 30%, which seems to be the maximum benefit achievable from annealing. A model explaining this interesting phenomenon has been postulated. Since annealing appeared to induce a structural reorganization by melting and recrystallization, both as-moulded and as-annealed PHB may be regarded as if crystallized from the melt at different undercoolings. Both initially possess a 'loose' amorphous phase. Subsequent ageing has been argued to be caused by the constraining effect of crystal perfection. The lamellar morphology in as-moulded PHB possesses a large specific crystalline–amorphous interface, perfection of which tightly constrains the amorphous phase between the crystals. Since annealing produces a coarser texture possessing less interface area, subsequent crystal perfection occurs to a smaller extent, yielding a less constrained amorphous phase. Consequently, more amorphous regions retain a high enough relaxation strength to allow the adjustment that is essential for rotation of the adjacent crystals, i.e. plastic deformation. It is this ability to undergo plastic deformation that provides annealed PHB with toughness.

Notably, in many studies the melting point of PHB has been suggested to be ca. 175°C. In contrast, results from this study suggest that this temperature is related to the melting of crystals that have undergone rearrangement. The actual melting point of the initial crystal morphology may be considerably lower; e.g. when crystallized below 60°C, PHB may contain crystals with melting points ranging from 80 to 165°C. The structural reorganization upon annealing consists of melting and recrystallization, yielding a similar texture as would be

obtained when crystallized at the annealing temperature. In turn, this implies that the favourable texture may be established directly from the melt by moulding at high temperatures. This is impracticable, however, since the crystallization rate of PHB above 120°C is almost negligible, resulting in long crystallization times and degradation. In contrast, recrystallization above 120°C is rapid because annealing produces a well nucleated 'melt' due to the abundance of intact crystals and crystal residues.

A peculiarity that has not been addressed yet is the unique behaviour of PHB compared to other semicrystalline polymers with respect to the magnitude of its embrittlement. However, one should realize that annealed PHB shows rather common behaviour. It in fact resembles polypropylene with respect to its properties, ageing behaviour and morphology. Owing to its low nucleation density, however, PHB can be crystallized isothermally at large supercoolings and hence unusually fine morphologies can be achieved. For example, when crystallized below 60°C, PHB forms thin lamellar crystals possessing a core thickness of only 30 Å. Several other semicrystalline polymers, such as linear low-density polyethylene<sup>21</sup>, are also known to be capable of forming thin lamellae but always with a commensurate reduction of their crystallinity. This is not the case for PHB, which develops similar crystallinities at all supercoolings. Implicitly, as-moulded PHB possesses an exceptionally large crystalline–amorphous interface per unit volume. Any process involving this interface, such as perfection (i.e. ageing), will therefore be greatly pronounced compared to other semicrystalline polymers.

## REFERENCES

- 1 Anderson, A. J. and Dawes, E. A. *Microbiol. Rev.* 1990, **54**, 450
- 2 Dawes, E. A. and Senior, P. J. *Adv. Microbiol. Physiol.* 1973, **10**, 135
- 3 Barak, P., Coquet, Y., Halbach, T. R. and Molina, J. A. E. *J. Environ. Qual.* 1991, **20**, 173
- 4 Krupp, L. R. and Jewell, W. J. *Environ. Sci. Technol.* 1992, **26**, 193
- 5 Holmes, P. A. *Phys. Technol.* 1985, **16**, 32
- 6 Doi, Y., Kunioka, M., Nakamura, Y. and Soga, K. *Macromolecules* 1986, **19**, 1274
- 7 de Koning, G. J. M. and Lemstra, P. J. *Polymer* 1992, **33**, 3295
- 8 de Koning, G. J. M. and Lemstra, P. J. *Polymer* 1993, **34**, 4089
- 9 Holmes, P. A. 'Development in Crystalline Polymers' (Ed. D. C. Bassett), Vol. 2, Elsevier, London, 1988, p. 1
- 10 Doi, Y., et al., *Appl. Microbiol. Biotechnol.* 1988, **28**, 330
- 11 Organ, S. J. and Barham, P. J. *J. Mater. Sci.* 1991, **26**, 1368
- 12 Owen, A. J., Heinzl, J., Škrbić, Ž. and Divjaković, V. *Polymer* 1992, **33**, 1563
- 13 Barker, P. A. PhD Thesis, University of Bristol, 1993
- 14 Barham, P. J. *J. Mater. Sci.* 1984, **19**, 3826
- 15 Barham, P. J., Keller, A., Otun, E. L. and Holmes, P. A. *J. Mater. Sci.* 1984, **19**, 2781
- 16 Baltá-Calleja, F. J. and Vonk, C. G. 'X-Ray Scattering of Synthetic Polymers' (Ed. A. D. Jenkins), Elsevier, Amsterdam, 1989, pp. 247–303
- 17 Vonk, C. G. *J. Appl. Crystallogr.* 1975, **8**, 340
- 18 Ward, I. M. 'Mechanical Properties of Solid Polymers', Wiley-Interscience, London, 1971, pp. 107–9
- 19 Zachmann, H. G. and Wutz, C. *Polym. Prepr.* 1992, **33**, 261
- 20 Bowden, P. B. and Young, R. J. *J. Mater. Sci.* 1974, **9**, 2034
- 21 Defoor, F., et al., *Macromolecules* 1993, **26**, 2575